

The Very Near Pressure Field of Three-Stream Jets

A. Adam*, D. Papamoschou†, J. Xiong‡ and F. Liu§

University of California, Irvine, Irvine, CA, 92697, USA

Using large eddy simulation (LES) of a hot coaxial three-stream jet we assess key assumptions of a recent volumetric model of the jet noise source based on the Reynolds-Averaged Navier Stokes (RANS) flow field and explore the proper definition of a linear surface-based model. Direct evaluation of the Reynolds stress and convective velocity shows that the RANS-based outer surface of peak stress (OSPS) and convective velocity on this surface are in good agreement with the LES results. In addition, examination of the instantaneous LES pressure field indicates that the most energetic pressure events occur on the OSPS. These results lend credence to the use of the RANS-based OSPS to simulate the convective Mach number distribution in a multi-stream jet, one of the most critical decisions in the volumetric modeling. The effort on the surface-based model focuses on the proper location of the “radiator surface”, at the boundary between the rotational and irrotational fields, on which linear partial fields would represent the imprint of turbulent structures in the jet flow. Definitions of the radiator surface based on thresholds of the gradient of the mean axial velocity place the surface outside of the hydrodynamic/acoustic boundary as determined by space-time correlations of the pressure field, thus fail to produce a surface with the desired property. A surface on which the convective velocity is identical to that on the OSPS falls exactly on hydrodynamic/acoustic boundary. This surface also appears to follow the outer band of a layer of negative pressure skewness.

I. Introduction

The work presented in this report relates to the development of physics-based models for the jet noise source that can be used in low-cost prediction schemes. Low cost here means that the predictive methods are informed by Reynolds-Averaged Navier Stokes (RANS) solutions of the flow field. The focus is on three-stream jets at conditions relevant to variable-cycle engines for supersonic transports. The acoustics and fluid dynamics of these jets have received considerable attention in recent experimental and numerical studies.¹⁻⁴

Jet noise source modeling can take two forms, volumetric and surface-based. RANS-based volumetric source modeling for three-stream jets, in coaxial and asymmetric configurations, has underscored the importance of properly modeling the convective velocity U_c of the turbulent eddies that dominate sound production.⁵ Specifically, sound emission is thought to be strongly influenced by the dynamics of the outer shear layer of the multi-stream jet. In a time-averaged sense, the action of the eddies in the outer shear layer is represented by the local peak of the Reynolds stress, resulting in the definition of the outer surface of peak stress (OSPS). The mean axial velocity on this surface is set to represent U_c , and the axial convective Mach number, which controls the radiation efficiency, is defined accordingly.

Linear surface-based models have the advantage of allowing not only propagation but also scattering predictions using well-established techniques like the boundary element method; thus, they are able to address the acoustics of propulsion-airframe integration. See Fig. 1. The source is prescribed as random partial fields on a “radiator surface” at the boundary between the inner nonlinear rotational flow field and outer linear pressure field. It is on this surface that the linear pressure distribution reflects the “footprint” of the turbulence, and in particular the coherent structures that dominate mixing and noise generation.^{6,7} Each partial field is envisioned to be an amplitude modulated traveling wave with finite axial and azimuthal

*Graduate Student, Department of Mechanical and Aerospace Engineering, AIAA Member

†Professor, Department of Mechanical and Aerospace Engineering, Fellow AIAA

‡Post-Doctoral Researcher, Department of Mechanical and Aerospace Engineering, AIAA Member

§Professor, Department of Mechanical and Aerospace Engineering, Fellow AIAA

scales, reflecting the wavepacket nature of jet noise that has been the subject of numerous studies.^{8–11} As with the volumetric approach, modeling of the convective velocity U_c on the radiator surface is a critical element of the predictive scheme, and it is desired to inform this decision using the RANS flow field. In this vein, initial numerical studies in a single-stream jet have shown promise in connecting the properties of the linear partial fields to the statistics of the RANS flow field.¹² Extension of this approach to multi-stream jets presents several challenges that motivate the present study.

Here, the time-resolved numerical solution of an axisymmetric three-stream jet, obtained using large eddy simulation (LES), allows initial evaluation of key assumptions made in the aforementioned RANS-based volumetric modeling and addresses some of the challenges related to the definition of surface-based sources. For the volumetric model, we examine the validity of the OSPS-based definition of U_c by evaluating the Reynolds stress directly and computing the convective velocity using space-time correlations. For the surface-based modeling, we assess various definitions of the radiator surface and connect its location to the statistics of the pressure field.

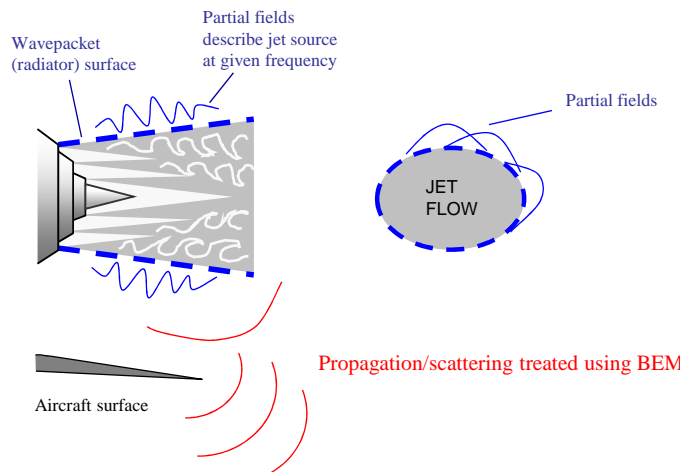


Figure 1. Basic elements of surface-based modeling of the jet noise source.

II. Jet Flow

We will analyze the jet flow from a three-stream, axisymmetric nozzle whose shape and coordinates are depicted in Fig. 2. Past reports have provided details on this nozzle design, called AXI04U, and its evolution from earlier axisymmetric designs.^{5,13} The subscripts p , s , and t will refer to the primary (inner), secondary (middle), and tertiary (outer) streams, respectively. Nozzle AXI04U has secondary-to-primary area ratio $A_s/A_p = 1.44$, and tertiary-to-primary area ratio $A_t/A_p = 1.06$. In its subscale experimental implementation, it had a tertiary exit diameter $D_t=38.1$ mm and an effective (area-based) primary diameter $D_{p,\text{eff}} = 13.33$ mm. It was operated at the cycle conditions listed in Table 1, which represents exhaust conditions for a supersonic turbofan engine at takeoff. The symbol U refers to the exit (fully-expanded) velocity; the nozzle pressure ratio (NPR) is the ratio of the jet stagnation pressure to ambient pressure; the nozzle temperature ratio (NTR) is the ratio of the effective (density based) jet stagnation temperature to ambient temperature; and the bypass ratio (BPR) is the ratio of either secondary or tertiary stream mass flow rate to the primary stream mass flow rate. The Reynolds number based on the conditions of the primary stream and $D_{p,\text{eff}}$ was 1.8×10^5 .

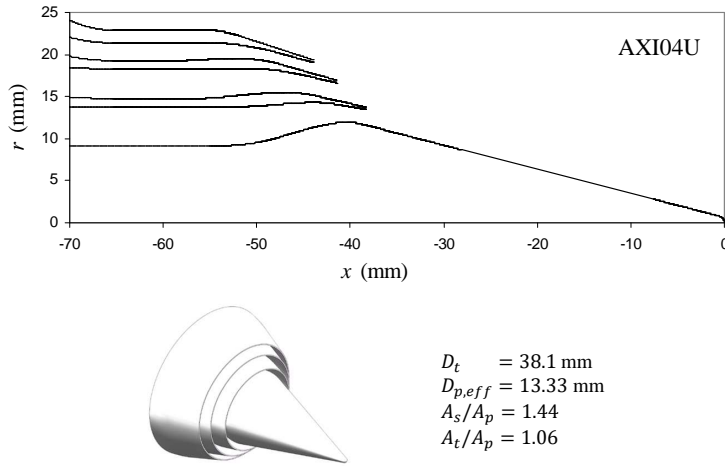


Figure 2. Dimensions of nozzle AXI04U.

Primary			Secondary				Tertiary			
NPR_p	NTR_p	U_p , m/s	BPR_s	NPR_s	NTR_s	U_s/U_p	BPR_t	NPR_t	NTR_t	U_t/U_p
2.02	3.38	590	2.33	2.02	1.34	0.63	1.31	1.53	1.24	0.48

Table 1. Cycle point.

III. Computational Details

Two types of computations were applied to jet AXI04U: Reynolds-Averaged Navier Stokes (RANS) and Large Eddy Simulation (LES). Both were conducted at the cycle conditions listed in Table 1 and at the Reynolds number of the subscale experiments. The axial and radial coordinates are x and r , with $x = 0$ indicating the tip of the primary plug. Below we summarize the main elements of the numerical codes.

A. RANS

The computational fluid dynamics code used in this project is known as PARCAE,¹⁴ which has been applied to similar nozzles.^{3,15} The code solves the unsteady three-dimensional Navier-Stokes equations on structured multiblock grids using a cell-centered finite-volume method. Information exchange between multiblock grids is implemented through MPI (Message Passing Interface) protocol. A time-averaged implementation of this code is used on this work, where it solves the RANS equations using the Jameson-Schmidt-Turkel dissipation scheme¹⁶ and the Shear Stress Transport (SST) turbulence model of Menter.¹⁷ The governing equations were solved explicitly in a coupled manner using five-stage Runge-Kutta scheme toward steady state with local time stepping, residual smoothing, and multigrid techniques for convergence acceleration. Only the steady-state solution was considered because we are interested in the time-averaged features of the flow.

The computation encompassed both the internal nozzle flow as well as the external plume. The computational domain extended to $30D_t$ axially and $8D_t$ radially. In order to save computational resources, the symmetry of the flow was used and only one half of it was simulated. For all three streams, uniform total pressure was specified at the inlet surface corresponding to a perfectly expanded exit Mach number. For the ambient region surrounding the nozzle flow, a characteristic boundary condition was defined, and the downstream static pressure was set equal to the ambient pressure. Adiabatic no-slip boundary condition was specified on all nozzle walls. The grid contained around 8 million points.

The code has been validated against mean velocity measurements under cold conditions.¹⁸ Cold-flow comparisons for three-stream jets similar to the one discussed here have shown similar level of agreement.

B. LES

For the LES, The PARCAE solver discussed above was used in its unsteady implementation. The solver uses implicit backward three-layer second-order time integration with explicit five stage Runge-Kutta dual time stepping. The spatial discretization of the inviscid flux is based on the weighted averaged flux-difference splitting algorithm of Roe.^{19,20} The viscous flux is discretized using a second-order central difference scheme. The time-evolving jet flow is simulated using a hybrid RANS/LES approach.²¹ Near the wall region the Spalart-Allmaras turbulence model²² is used to model the turbulent viscosity, while in the free shear flow the computation relies on the subtle dissipation of the upwind scheme, using the method proposed by Shur *et al.*²⁰

The computational grid extended $60D_t$ in the axial direction and $20 D_t$ in the radial direction; it contained approximately 40 million elements. For each nozzle flow, it was imposed a perfectly expanded exit, with constant total pressure, total temperature, and zero flow angle. For the ambient region surrounding the nozzle flow, a non-reflecting characteristic boundary condition was imposed, and a buffer layer was implemented near the outflow. An adiabatic no-slip boundary condition was specified on the nozzle wall. The computation included the internal nozzle and external plume. Figure 3 shows the mesh used, as well as example vorticity and pressure contours of the computation.

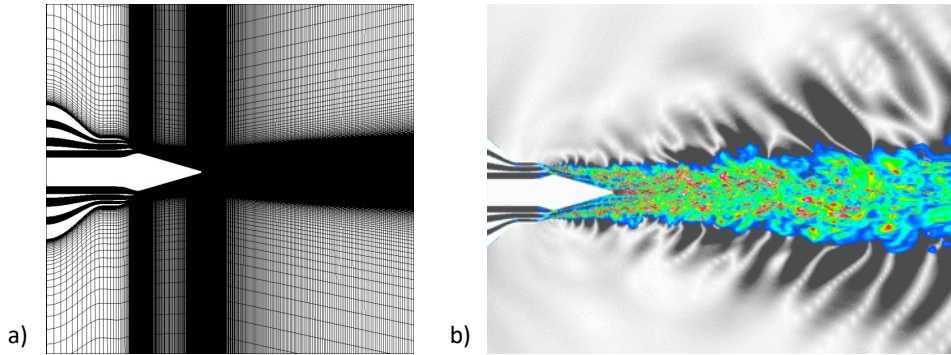


Figure 3. a) LES computational mesh; b) LES instantaneous fields, with inner region showing vorticity contours and outer region plotting the magnitude of the pressure fluctuation,, $|p'/p_\infty| < 0.004$.

The LES results reported here represent 885 time steps of separation $\Delta t = 5 \times 10^{-6} s$. To improve the accuracy of the statistics, azimuthal averaging at six meridional planes, separated by 60° , was applied. This is justified by the fact that the azimuthal coherence at separation of 60° is very weak,²³ essentially making each meridional plane statistically independent.

IV. Comparison of RANS and LES Flow Fields

We examine the distributions of the mean axial velocity and the principal component of the Reynolds stress tensor, as computed by each technique. The importance of the Reynolds stress in the modeling of the noise source in multi-stream jets was emphasized in Ref. 5. Following that work, the principal component of the Reynolds stress is defined as

$$g = | \langle u'q' \rangle | \quad (1)$$

where u' is the axial velocity fluctuation, q' is the transverse velocity fluctuation in the direction of the mean velocity gradient, and $\langle \rangle$ denotes the time average. For the LES, g is calculated directly from the time resolved data. For RANS, it is given by

$$g = \nu_T G \quad (2)$$

where ν_T is the turbulent viscosity and G is the magnitude of the mean velocity gradient. For the remainder of the report, g will be loosely referred to as the ‘‘Reynolds stress’’.

Figure 4 plots contours of the mean axial velocity normalized by the primary exit velocity, \bar{u}/U_p , on the plane of symmetry and compares the RANS and LES predictions. The two flow fields are very similar, with the LES predicting slightly faster spreading and thus moderately smaller potential core. It is also noted that the wake from the plug is accentuated in the RANS simulation. Figure 4 also indicates that the LES provides a fairly stable result for the mean velocity despite the relatively small number of time steps.

The analogous comparisons for the Reynolds stress are given in Fig. 5. Here we note that the LES results have not fully converged, being fairly stable for $x/D_t \leq 7$ but unstable (and unreliable) downstream. Also, note that g contours for LES were averaged onto a half plane and reflected to show the effect of the full jet. Within the region $x/D_t \leq 7$, the comparison between RANS and LES is very good both in terms of levels and shapes of the distributions.

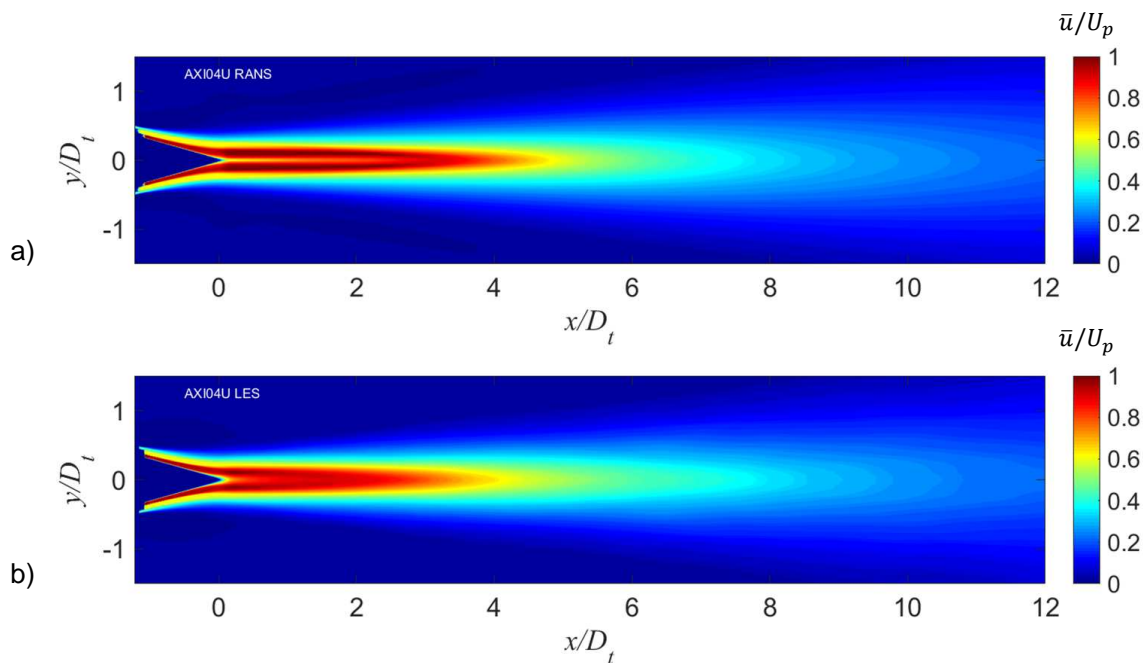


Figure 4. Contour plots of normalized mean axial velocity \bar{u}/U_p . a) RANS and b)LES.

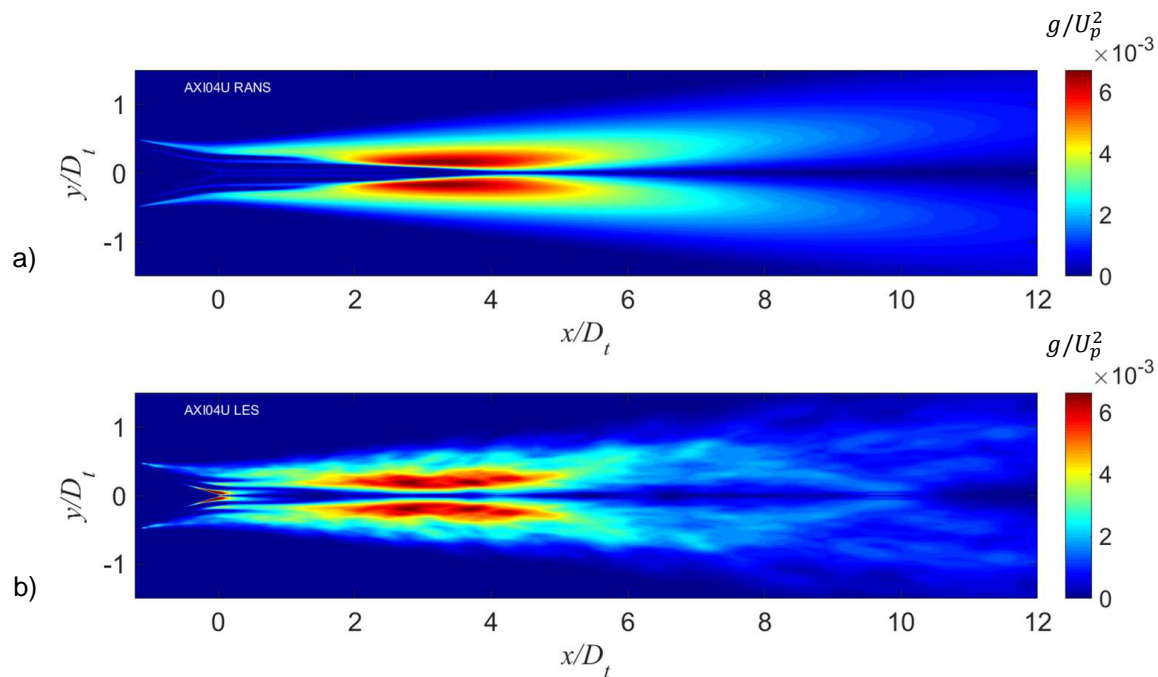


Figure 5. Contour plots of Reynolds stress g/U_p^2 . a)RANS and b)LES.

V. Outer Surface of Peak Stress

In the acoustic analogy model of Ref. 5 it was surmised that, in multi-stream jets, the turbulent eddies in direct contact with the ambient are the principal noise generators. In a three-stream jet like the one considered here, these eddies are initially in the tertiary (outer) shear layer, then progressively transition to the secondary and primary shear layers as the tertiary and secondary flows become mixed with the primary flow. In the context of RANS, the action of those eddies is represented by the statistics on the outer-most peak of the Reynolds stress g , that is, the first peak of g as one approaches the jet radially from the outside towards the inside. This results in the concept of the “outer surface of peak stress” (OSPS), which is thought to be important in the understanding and modeling of multi-stream jet noise. Among the most important properties of the eddies in contact with the ambient is their convective velocity U_c or convective Mach number $M_c = U_c/a_\infty$. The convective Mach number governs the efficiency with which the eddies radiate sound to the far field, it is thus of paramount significance in the modeling. Here we have an opportunity to test certain assumptions used in the RANS-based modeling of U_c by obtaining direct results from the LES.

The detection for the OSPS is similar for both RANS and LES, and follows the general procedure outlined in Ref. 5. It is summarized here briefly, with Fig. 6 illustrating the basic procedure. The flow field is divided into axial slices of very fine spacing near the nozzle exit and coarser spacing downstream. For RANS, each axial slice is divided into fine azimuthal segments, typically in 2.5-degree increments. The LES results were provided on meridional planes. Within each azimuthal segment or plane, the data (velocity, Reynolds stress) are sorted in order of the decreasing radius r . The search process for the first (outermost) peak of the Reynolds stress starts at the radial location where the mean axial velocity is one third of the tertiary exit velocity, a position that is well outside the dividing streamline of the outermost shear layer but still within the jet flow. Starting the search within the jet flow prevents spurious detection of peaks that may occur if one started the search further out where the velocity is very low and the data can be noisy. Denoting g_j the discrete values of the Reynolds stress, the operation $h_j = \max(g_j, g_{j+1})$ is carried out as we move inward towards the jet axis. We seek the first occurrence where h_j remains invariant for M_{zero} consecutive points. This indicates that the first peak of the Reynolds stress occurred at point $j - M_{zero}$. It is clear that, beyond the ends of the secondary and tertiary shear layers, there is no distinction between the outer peak and the global peak of g on a given meridional plane.

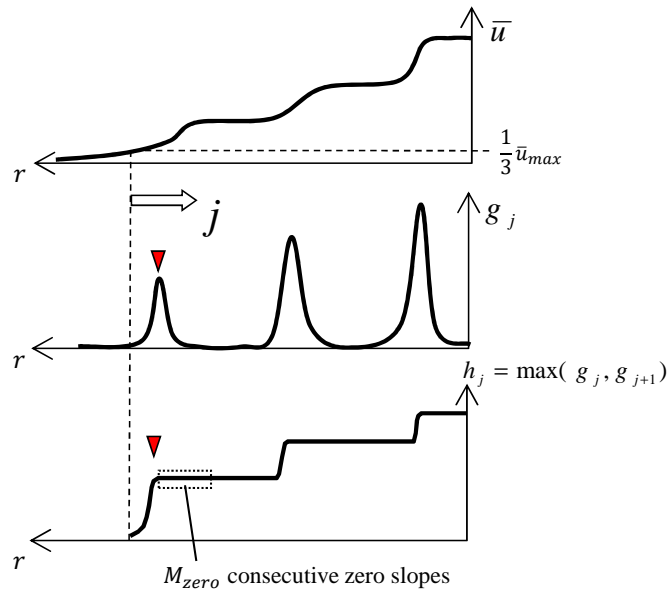


Figure 6. Detection scheme for locating the outer surface of peak stress.

A. OSPS Based on RANS

For the RANS computation, once the OSPS has been detected, the convective velocity U_c is modeled as the mean axial velocity on the OSPS. Denoting the radius of the OSPS as $r_{OSPS}(x)$, the convective velocity is modeled as

$$U_c(x) = \bar{u}(x, r_{OSPS}(x)) \quad (3)$$

Figure 7 plots a three-dimensional view of the OSPS of jet AXI04U. The color contours on the surface represent the convective Mach number M_c . The OSPS experiences a sudden convergence where the outer streams become totally mixed with the primary shear layer. This is followed by a gradual convergence near the end of the primary potential core, downstream of which the OSPS diverges slowly.

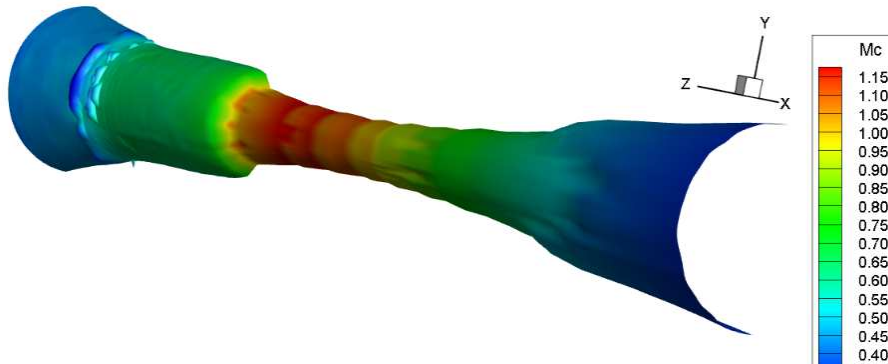


Figure 7. M_c distribution on OSPS surface.

B. OSPS based on LES

Because of the inherent noise of LES results and the fact that the data is only stored in azimuthal planes, the treatment of the OSPS based on this data needs to follow a different procedure. The detection scheme is applied to six meridional planes at azimuthal angles $\phi = 0^\circ$ to 300° in increments 60° . The OSPS is located

on each plane and the convective velocity is computed along each OSPS following the procedure outlined below. The final result is the average of all six distributions of peak stress locations and convective velocities.

The LES solution allows calculation of the space-time correlation anywhere within the computational domain. For a given azimuthal angle, the axial space-time correlation of the axial velocity fluctuation u' , in normalized form, is

$$R_{uu}(x, r; \xi, \tau) = \frac{\langle u'(x, r, t)u'(x + \xi, r, t + \tau) \rangle}{u'_{rms}(x, r)u'_{rms}(x + \xi, r)} \quad (4)$$

where rms denotes the root mean square. A similar formulation is used for R_{pp} , the space-time correlation of p' . Examples of space-time correlations are plotted in Fig. 8.

Computation of the convective velocity at a given point of the computational grid involved space-time correlations at small axial separations around this point, with minimum correlation of 0.4. Because each correlation function comprises a discrete set of points, to accurately locate the maximum value of the correlation at axial separation ξ_i a seventh-order polynomial was fitted around the peak of the correlation curve (dashed lines in Fig. 8). The time separation τ_i corresponding to the maximum value of the polynomial (i.e., the root of the derivative) was then calculated using a Newton-Raphson iteration method. The convective velocity for this axial separation is $U_{c,i} = \xi_i/\tau_i$ and the overall U_c at point (x, r) was obtained by averaging $U_{c,i}$ over the separations that satisfied $R_{uu_{max}} > 0.4$.

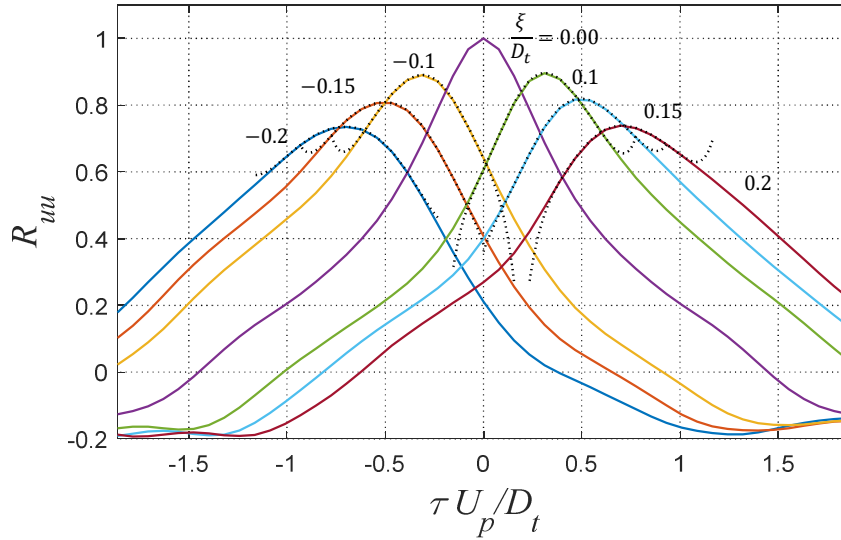


Figure 8. Space-time correlation R_{uu} on the OSPS at $x/D_t = 1.0$. Dashed lines indicate fits by seventh-order polynomials to accurately detect the peak of each correlation.

C. Comparisons of RANS and LES Results

We proceed with comparing the OSPS location, and U_c distribution on the OSPS, for the RANS and LES methods discussed above. Figure 9 plots the radial coordinates of the OSPS for RANS and LES. The two surfaces are practically identical up to $x/D_t = 2$, with the plot showing clearly the inward transition of the OSPS from the tertiary to the secondary to the primary shear layer. For $2 \leq x/D_t \leq 7$, the two surfaces are close but the LES result is shifted outward, reflecting the more rapid spreading of the LES jet. As discussed earlier, Reynolds stress results for $x/D_t > 7$ are unreliable because of the limited number of samples.

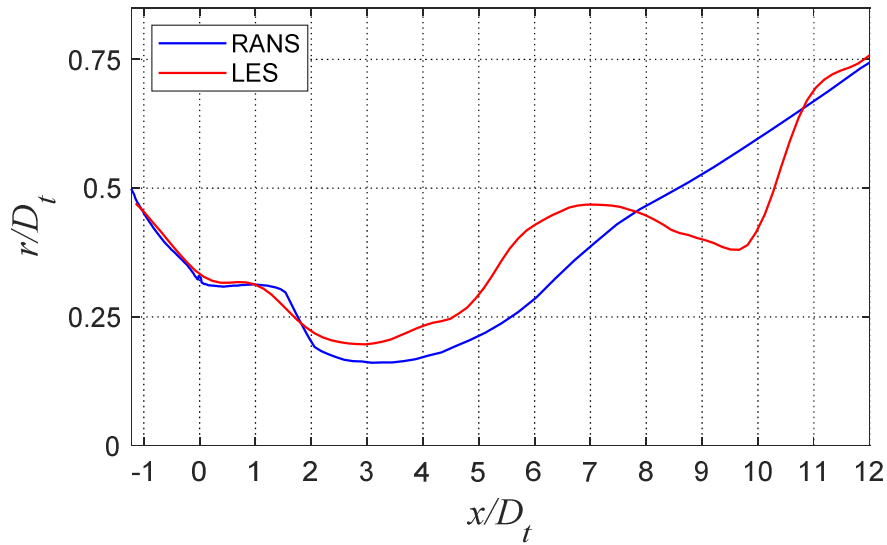


Figure 9. OSPS distribution for RANS and LES.

The comparison of convective velocities on the OSPS is seen in Fig. 10. The RANS- and LES-based trends are similar and show the increase in U_c as the most energetic eddies move from the tertiary (low speed) to the secondary (medium speed) to the primary (high speed) shear layer, followed by a decline in U_c as the mean velocity decays past the end of the primary potential core. There are moderate quantitative differences between the RANS and LES results, with RANS predicting a peak value of U_c that is about 10% higher than that predicted by LES. Overall, the comparison provides encouragement that the RANS flow field can yield a fairly accurate convective velocity distribution for the purposes of jet noise modeling.

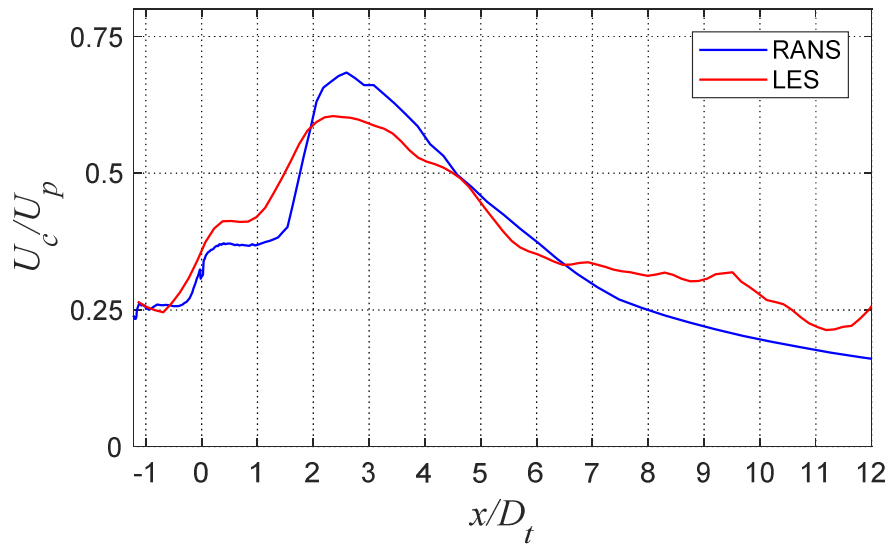


Figure 10. U_c distribution for RANS and LES along their respective OSPS.

VI. Radiator Surface

The radiator surface is a concept introduced in earlier studies of single- and dual-stream jets.^{12,23} It is defined as the closest surface to the jet centerline on and outside of which the propagation of pressure perturbation is governed by the homogeneous linear wave equation. It is on this surface that a linear model for jet noise, in the form of wavepackets, could be informed by turbulent statistics computed by low-cost methods such as RANS. As we move away from this surface, the hydrodynamic information is lost rapidly. One of the most important elements of a surface source model is the convective velocity U_c . Although this connection has been explored with some promise in round single-stream jets,¹² multi-stream jets present several challenges for the proper definition of the radiator surface.

Following the analysis of Papamoschou *et al.*,¹² the criterion for the location of the radiator surface in a single-stream jet can be formed as

$$\frac{\partial\bar{u}/\partial r}{(\partial\bar{u}/\partial r)_{max}} \rightarrow 0 \quad (5)$$

Accordingly, the edge $r_{edge}(x)$ is defined as the radial position where the radial gradient of the mean axial velocity, normalized by its local peak value, equals a given threshold $\kappa \ll 1$:

$$\frac{|\partial\bar{u}/\partial r|(x, r_{edge}(x))}{|\partial\bar{u}/\partial r|_{max}(x)} = \kappa \quad (6)$$

The usual threshold selected is $\kappa = 0.01$. For a multi-stream jet, one may select $|\partial\bar{u}/\partial r|_{max}(x)$ to be the outermost peak of the mean velocity gradient, similar to the definition of the OSPS in Section V.

There are several challenges with this definition of radiator surface. Accurate measurement of the mean velocity gradient at the edge of the jet is very difficult experimentally as the results can be quite noisy; the threshold κ in Eq. 6 is somewhat arbitrary and the placement of the radiator surface could be sensitive on its selection; and, for multi-stream jets, the proper gradient in the denominator of Eq. 6 is not clear. In the following sections, the location using the definition of Eq. 6 and its validity are discussed. Alternative definitions are contemplated, although a definitive practical definition remains a target for future efforts.

A. Location of the Radiator Surface

The location of the radiator surface is computed using the same kind of algorithm used for the detection of the OSPS, explained in section V. In order to find the outermost peak of $|\partial\bar{u}/\partial r|$, the search process starts radially from outside the flow to inside. Once found, the search goes in reverse to locate the edge of the jet using the threshold set by Eq. 6.

The choice of defining $|\partial\bar{u}/\partial r|_{max}(x)$ in Eq. 6 as the outermost peak, instead of the absolute peak, stems from the assumption that the outer shear layer dominates sound production. However, from a practical standpoint, use of the absolute maximum of $|\partial\bar{u}/\partial r|$ may be more convenient. We plot the result of the two definitions in Fig. 11. We note slight differences of the two surfaces up to $x/D_t = 1.5$, beyond which the two surface coincide as the outer shear layers vanish. The small difference upstream is explained by the fact that the profile of mean velocity at the first stages of the flow is very steep. Therefore, the velocity gradient decreases so fast outside the flow that it reaches both threshold values almost at the same position. It is also interesting to note that the OSPS ‘collapse’, at the end of the outer shear layers, begins at the union of the curves of peak $|\partial\bar{u}/\partial r|$.

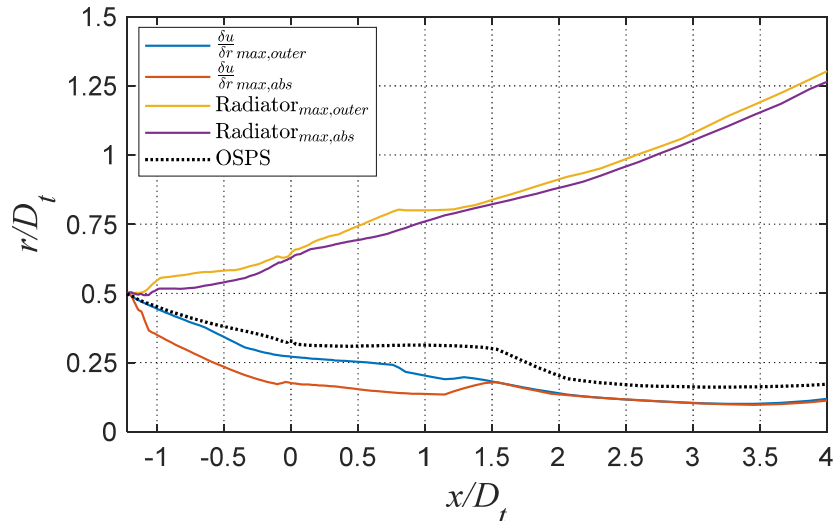


Figure 11. Comparison of radiator surfaces, using the outermost or absolute peak of $|\partial\bar{u}/\partial r|$.

B. Distribution of Convective Velocity

We seek a connection between the convective velocity distributions on the OSPS and on the edge of the jet. To this end, we plot contours of U_c/U_p on the $x-r$ plane in Fig. 12. In Fig. 12a U_c is based on the space-time correlation of u' (R_{uu}), and in Fig. 12b it is based on the space-time correlation of p' (R_{pp}). The former is relevant inside the vortical field, where the turbulent structures affect the velocity of the flow directly. The latter makes more sense when analyzing the outer flow, around the edge of the jet, where we seek the pressure imprint of the vortical eddies. The two distributions are similar, with an important distinction that will be discussed in the following. At a given axial location, U_c has a radial trend whereby it decreases outside the OSPS (depicted as red line), reaches a minimum, then rises sharply. The sharp rise is associated with the transition from the hydrodynamic to the acoustic field and the fact that acoustic disturbances can travel at large angles to the jet axis. This transition is faster in the case of the R_{pp} -based U_c . The overall trends are similar to those noted in a single-stream jet.¹² The RANS-based radiator surface, as defined by the criterion of Eq. 6 (dashed black line), falls marginally within the acoustic field for the R_{uu} -based distribution and well inside the acoustic field for the R_{pp} -based distribution. Therefore, it is too far outside the edge of the jet to properly satisfy its intended role. A consequence of this is that the convective velocity on the radiator surface, as defined by Eq. 6, does not match the convective velocity on the OSPS.

We now pose the reverse question: What is the shape of the surface, near the edge of the jet, where the U_c distribution matches that on the OSPS? The result is the white line in Fig. 12, which for brevity we designate as “ U_c -match”. It appears to track perfectly the hydrodynamic-acoustic transition of the R_{pp} -based U_c map, but is well inside the hydrodynamic region of the R_{uu} -based U_c map. The smoothness of the U_c -match line, and its proximity to the hydrodynamic/acoustic boundary in the R_{pp} -based U_c , suggests that the U_c information on the OSPS is transmitted to the jet rotational/irrotational boundary as determined by space-time correlations based on p' . This provides encouragement that there is a surface, having the desired properties of the radiator surface, on which the RANS-derived convective velocity (on the OSPS) would inform the definition of the partial fields. At this point, however, there is no direct indication how to accurately compute this boundary based on RANS information alone.

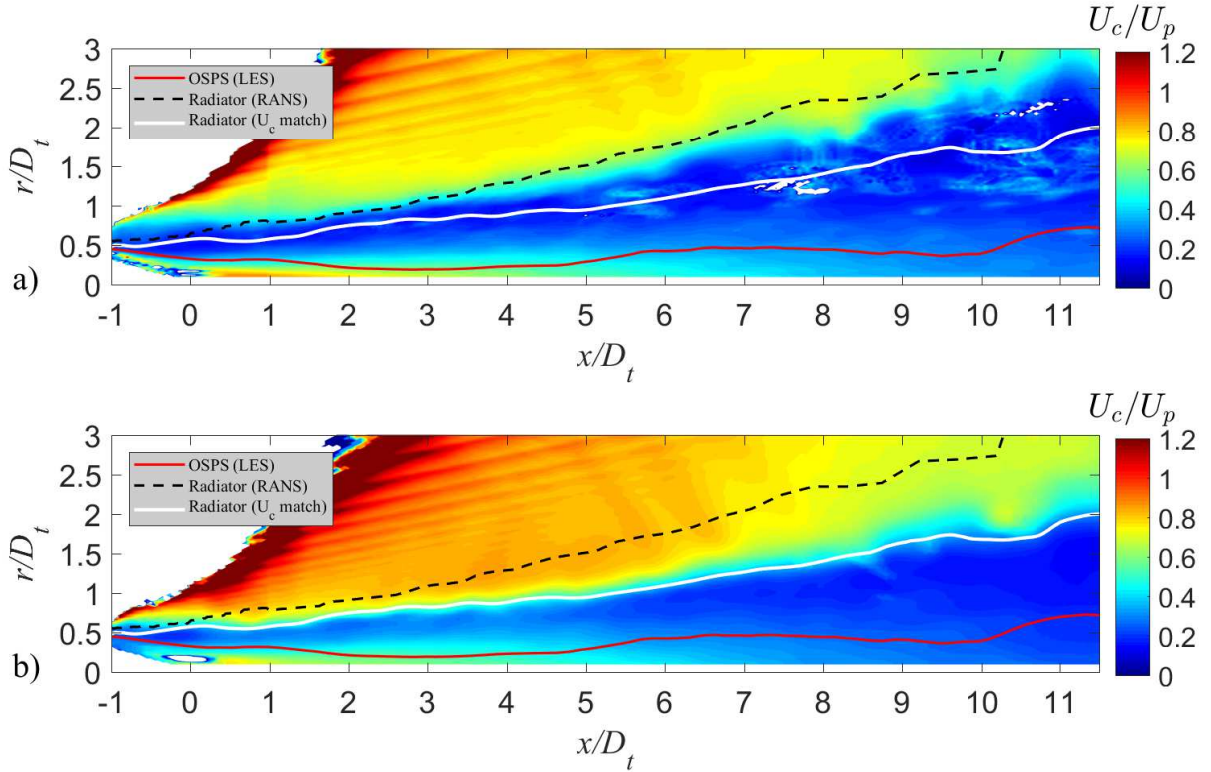


Figure 12. Distribution of normalized convective velocity U_c/U_p as determined by space-time correlations a) based on u' and b) based on p' . Red line: OSPS surface based on LES; black dashed line: classic definition of radiator surface; white line: radiator surface based on U_c -match criterion.

C. Distribution of Skewness of Pressure Field

An intriguing finding of earlier studies on the near pressure field of cold single- and dual-stream jets is the presence of a negative layer of skewness of p' near the edge of the jet.²³ Defining the normalized skewness as

$$Sk = \frac{\langle p'^3 \rangle}{\langle p'^2 \rangle^{3/2}} \quad (7)$$

the earlier studies found the radiator surface, as defined by Eq. 6 (with $\kappa = 0.01$), was practically coincident with the locus of $Sk \approx -0.3$. We are thus motivated to examine whether similar trends hold in the case of the hot three-stream jet.

Figure 13 presents contour maps of the pressure skewness distribution on the $x - r$ plane. There is definitely a negative skewness layer near the edge of the jet. The radiator surface, as determined by the U_c -match criterion discussed above (white line), appears to track the outer band of the negative skewness layer. On the other hand, the radiator surface as computed by the conventional means (dashed black line) is located well outside the negative skewness layer. Figure 14 plots the axial distribution of Sk along the U_c -match radiator. It is seen that the values are consistently negative, ranging from -0.1 to -1. The trend is noisy because of the relatively small number of steps in the LES computation, and the overall value of Sk along the radiator surface is lower than the previously proposed criterion of $Sk \approx -0.3$. Nevertheless, this result, in combination with the findings of the previous studies, indicates that the negative skewness layer is an important feature of the pressure field that deserves further study.

There are some additional features of interest in the skewness map of Fig. 13. In the acoustic field, we note positive values of skewness that suggest Mach wave radiation.²⁴ Inside the jet, we note a layer of slightly positive skewness that appears to follow the OSPS. The latter result is spotty and needs to be verified by longer-time integration.

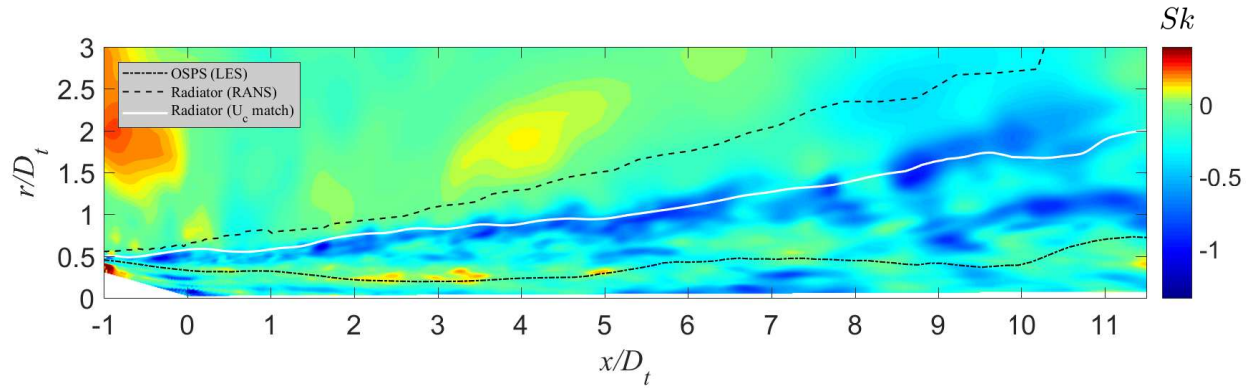


Figure 13. Distribution of normalized skewness of pressure field. Red line: OSPS surface based on LES; black dashed line: classic definition of radiator surface; white line: radiator surface based on U_c -match criterion.

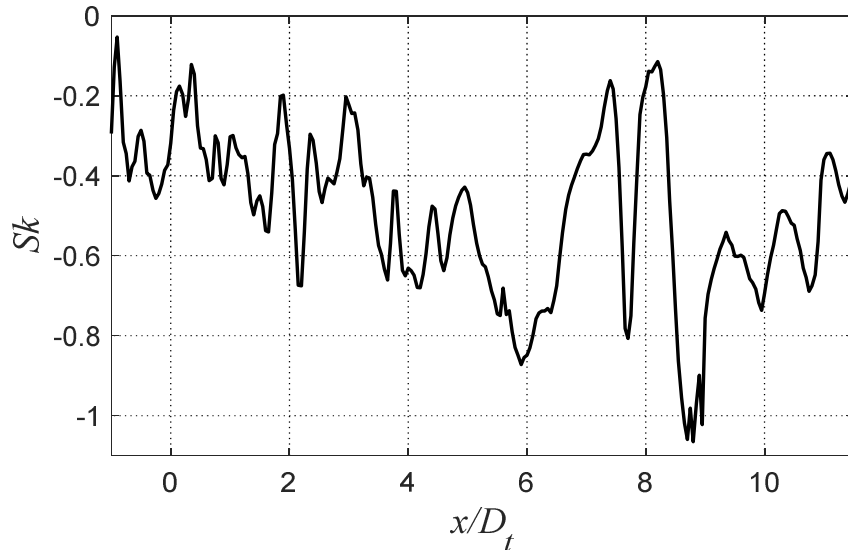


Figure 14. Distribution of Sk along radiator surface based on U_c -match criterion.

D. Distribution of Instantaneous Pressure Fluctuation

Given that the ultimate goal of this effort is prediction of acoustic radiation, it is interesting to visualize a “raw” result of the LES and examine how the various surfaces defined here (OSPS, radiator) may fit with this result. Specifically, we wish to visualize the magnitude of the instantaneous pressure fluctuation p' on the cross-sectional plane $\phi = 0^\circ$ throughout the domain of interest. Because of the large dynamic range of p' , it is convenient to present the result in the logarithmic form

$$\ln\left(\frac{|p'|}{p'_{rms,max}}\right)$$

where $p'_{rms,max}$ is the maximum rms pressure fluctuation in the domain. The related contour map is presented in Fig. 15 where the limits correspond to the range $10^{-4} \leq |p'|/p'_{rms,max} \leq 1$. Overlaid on the map are the coordinates of the OSPS and radiator surface based on the U_c -match criterion. These surfaces were computed by time averaging on the plane $\phi = 0^\circ$ only. Inside the jet, the most energetic pressure events appear to line up with the OSPS, indicating the value of this surface in jet noise modeling. Outside the

radiator surface, we observe a clear pattern of Mach waves radiating at the polar angle of peak emission which for this jet is around 30° relative to the jet axis.

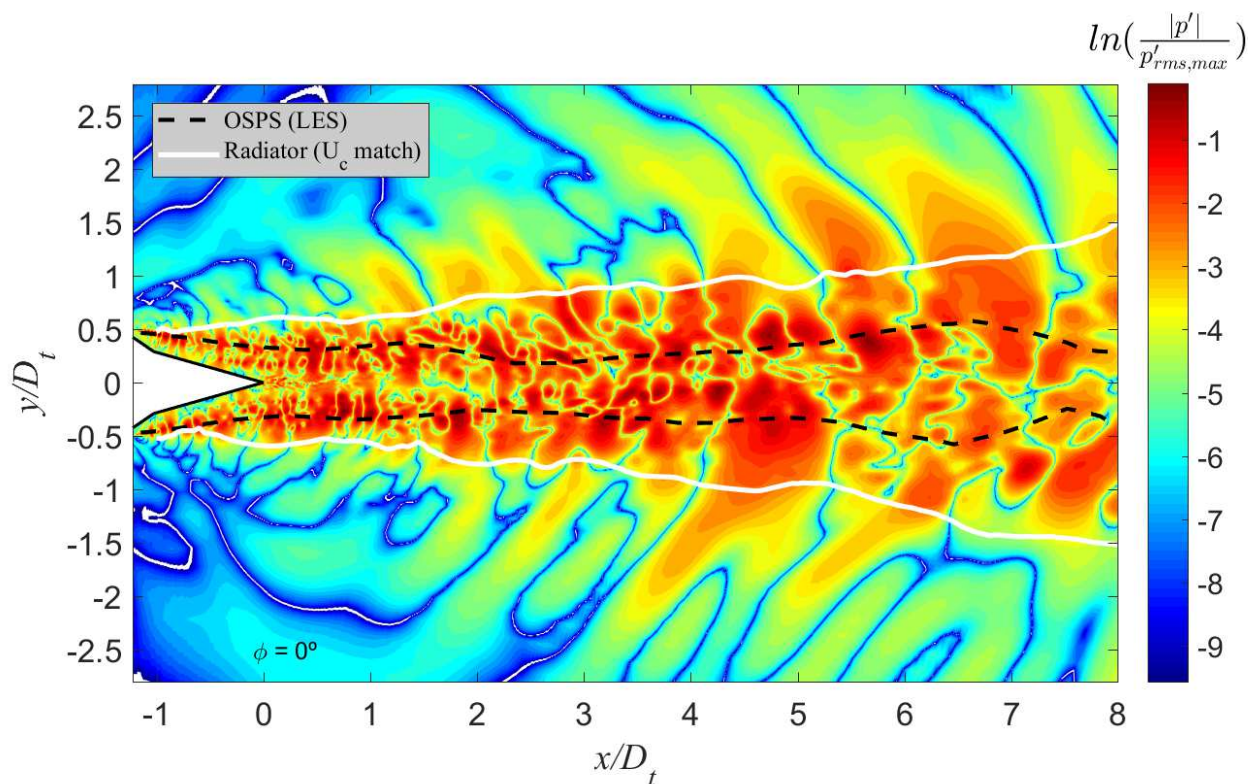


Figure 15. Distribution of the magnitude of the instantaneous pressure fluctuation, presented in normalized logarithmic form.

VII. Concluding Remarks

Using large eddy simulation (LES) of a hot coaxial three-stream jet, we assessed key assumptions used in recent RANS-based volumetric modeling of the jet noise source and explored the proper definition of a linear surface-based model. Direct evaluation of the Reynolds stress and convective velocity shows that the RANS-based outer surface of peak stress (OSPS) and convective velocity on this surface are in good agreement with the LES results. In addition, examination of the instantaneous LES pressure field indicates that the most energetic pressure events occur on the OSPS. These results lend credence to the use of the RANS-based OSPS to simulate the convective Mach number distribution in a multi-stream jet, one of the most critical decisions in the volumetric modeling.

The effort on the surface-based model focuses on the proper location of the “radiator surface”, at the boundary between the rotational and irrotational fields, on which linear partial fields would represent the imprint of turbulent structures in the jet flow. To this end, we computed the convective velocity U_c throughout the symmetry plane using space-time correlations of u' and p' . Both U_c fields show a sharp transition between hydrodynamic and acoustic fields, thus defining the “edge” of the jet, with the edge based on u' occurring outward relative to the edge based on p' . Definitions of the radiator surface based on thresholds of the gradient of the mean axial velocity place the surface outside of both edges, thus fail to produce a surface with the desired property. A surface on which U_c is identical to that on the OSPS falls exactly on the edge of the jet based on the p' space-time correlation. This surface also appears to follow the outer band of a layer of negative pressure skewness, as has been observed in a cold single-stream jet.²³ Although an exact definition of the radiator surface for multi-stream jets remains under investigation, the elements presented here offer intriguing prospects for further study of the phenomena at the edge of the multi-stream jet.

Acknowledgments

The support by NASA Cooperative Agreement NNX14AR98A, monitored by Dr. James Bridges, is gratefully acknowledged.

References

- ¹Henderson, B., “Aeroacoustics of Three-Stream Jets,” *AIAA Paper 2012-2159*, June 2012.
- ²Henderson, B., Leib, S., and Wernet, M., “Measurements and Predictions of the Noise from Three-Stream Jets,” *AIAA Paper 2015-3120*, Jan. 2015.
- ³Papamoschou, D., Phong, V., Xiong, J., and Liu, F., “Quiet Nozzle Concepts for Three-Stream Jets,” *AIAA Paper 2016-0523*, Jan. 2016.
- ⁴Huff, D. and Henderson, B., “The Aeroacoustics of Offset Three-Stream Jets for Future Commercial Supersonic Aircraft,” *AIAA Paper 2016-2992*, June 2016.
- ⁵Papamoschou, D., “Modelling of Noise Reduction in Complex Multistream Jets,” *Journal of Fluid Mechanics*, Vol. 834, Jan. 2018, pp. 555–559.
- ⁶Ho, C., “Near Field Pressure Fluctuations in a Circular Jet,” *NASA CR-179847*, Nov. 1985.
- ⁷Zaman, K., “Flow Field and Near and Far Sound Field of a Subsonic Jet,” *Journal of Sound and Vibration*, Vol. 106, No. 1, 1986, pp. 1–16.
- ⁸Morris, P., “A Note on Noise Generation by Large Scale Turbulent Structures in Subsonic and Supersonic Jets,” *International Journal of Aeroacoustics*, Vol. 8, No. 4, 2009, pp. 301–316.
- ⁹Reba, R., Narayanan, S., and Colonius, T., “Wave-Packet Models for Large-Scale Mixing Noise,” *International Journal of Aeroacoustics*, Vol. 9, 2010, pp. 533–558.
- ¹⁰Papamoschou, D., “Wavepacket Modeling of the Jet Noise Source,” *AIAA Paper 2011-2835*, June 2011.
- ¹¹Jordan, P. and Colonius, T., “Wave Packets and Turbulent Jet Noise,” *Annual Review of Fluid Mechanics*, Vol. 45, 2013, pp. 173–195.
- ¹²Papamoschou, D., Xiong, J., and Liu, F., “Towards a Low-Cost Wavepacket Model of the Jet Noise Source,” *AIAA Paper 2015-1006*, Jan. 2015.
- ¹³Phong, V. and Papamoschou, D., “Investigation of Isolated and Installed Three-Stream Jets from Offset Nozzles,” *AIAA Paper 2017-0005*, Jan. 2017.
- ¹⁴Xiong, J., Johnson, A., Liu, F., and Papamoschou, D., “Body Force Model for the Aerodynamics of Inclined Perforated Surfaces,” *AIAA Journal*, Vol. 50, No. 11, 2012, pp. 2525–2535.
- ¹⁵Papamoschou, D., Xiong, J., and Liu, F., “Reduction of Radiation Efficiency in High-Speed Jets,” *AIAA Paper 2014-2619*, June 2014.
- ¹⁶Jameson, A., Schmidt, W., and Turkel, E., “Numerical Solutions of the Euler Equations by Finite Volume Methods Using Runge-Kutta Time Stepping Schemes,” *AIAA Paper 1981-1259*, January 1981.
- ¹⁷Menter, F., “Two-Equation Eddy-Viscosity Turbulence Models for Engineering Applications,” *AIAA Journal*, Vol. 32, No. 8, 1994, pp. 1598–1605.
- ¹⁸Xiong, J., Nielsen, P., Liu, F., and Papamoschou, D., “Computation of High-Speed Coaxial Jets with Fan Flow Deflection,” *AIAA Journal*, Vol. 48, No. 10, 2010, pp. 2249–2262.
- ¹⁹Roe, P. L., “Approximate Riemann Solvers, Parameter Vectors and Difference Schemes,” *Journal of Computational Physics*, Vol. 46, No. 2, 1980, pp. 357–378.
- ²⁰Shur, M. L., Spalart, P. R., and Strelets, M. K., “Noise Prediction for Increasingly Complex Jets. Part I: Methods and Tests,” *International Journal of Aeroacoustics*, Vol. 4, No. 3, 2005, pp. 213–246.
- ²¹Spalart, P. R., Jou, W. H., Strelets, M., and Allmaras, S. R., “Comments on the Feasibility of LES for Wings, and on a Hybrid RANS/LES Approach,” 1st AFOSR Int. Conf. on DNS/LES, Ruston, LA, August 1997.
- ²²Spalart, P. R. and Allmaras, S. R., “A One-Equation Turbulence Model for Aerodynamic Flows,” *AIAA Paper 1992-0439*, January 1992.
- ²³Papamoschou, D. and Phong, V., “The Very Near Pressure Field of Single- and Multi-Stream Jets,” *AIAA Paper 2017-0230*, Jan. 2017.
- ²⁴Gee, K., Neilsen, T., and Atchley, A., “Skewness and Shock Formation in Laboratory-Scale Supersonic Jet Data,” *Journal of the Acoustical Society of America*, Vol. 133, May 2013, pp. 491–497.